Power Flow Control Using a DC-DC MMC for HVdc grid Connected Wind Power Plants

Ricardo Vidal, Enrique Belenguer
University of Jaume
Castellón, Spain
{rvidal,efbeleng}@uji.es

Diego Soto
University of Magallanes
Punta Arenas, Chile
diego.soto@umag.cl

Ramón Blasco-Gimenez
Technical University of Valencia
Valencia, Spain
r.blasco@ieee.org

Cristián Pesce
University of La Frontera
Temuco, Chile
cpesce@udec.cl

Rubén Pena
University of Concepción
Concepción, Chile
rupena@udec.cl

Javier Riedemann
University of Bío-Bío
Concepción, Chile
jriedema@ubiobio.cl

***Abstract* — This paper proposes the use of a transformer-less DC-DC Modular Multilevel Converter (MMC) topology, based on cascaded H-bridge converters, for power flow control in High Voltage Direct Current (HVDC) grids used to connect off-shore wind power plants to on-shore grids. An energy based approach is used to regulate the DC voltage of H-bridge modules. Results for the operation of the DC-DC MMC supplying energy to a DC network and controlling the power flow in a HVDC system are presented.**

***Index Terms*—Wind power generation, Power Control, HVDC converters, Modular multilevel converters.**

I. Introduction

HVDC grids will be used to deliver large amounts of renewable power from generation locations to consumption centers in Europe. Voltage Source Converters (VSC) based on Modular Multilevel topologies represent the current preferred technological option to connect large wind power plants (WPP) to HVDC grids. They have important technical advantages, such as, black-start operation of the off-shore grid and use of cheaper XLPE cable. VSC-HVDC grids could also contribute to enhance frequency and voltage stability of weak AC systems and prevent blackouts [1]–[3]. Multi-terminal HVDC configurations with more lines than converter stations require additional equipment for power flow control. Several alternatives have been proposed, including the use of DC-DC converters with high-frequency transformers and even the use of switchable resistors. These configurations have the drawbacks of requiring complex high voltage high frequency transformers, the former, and the increase in losses the latter.

The Modular Multilevel Converter topology has become very attractive high voltage, high power VSC-HVDC converter station [4]-[7]. The MMC typically uses a string of half or full bridge converter modules [7], offering advantages such as high quality voltage and current waveforms; low switching frequency, hence low power losses. Because of the building block simplicity, a highly modular design approach to meet the high voltage and power levels required for HVDC applications. Because of its advantages, the MMC is being considered for modular multilevel DC-DC conversion topologies such as those proposed in [8]-[12].

This technology may be suitable to interconnect HVDC systems by their DC sides so as to implement a HVDC grid [13]-[14]. The topology in [8] and [9] is basically a cascade of two standard AC-DC MMC stages which are connected by its AC sides. The first MMC implements the DC-AC conversion stage, of moderate frequency, whereas the second MMC implements the AC-DC conversion stage. A similar alternative but based on the Alternating Arm Converter (AAC) is proposed in [10]. Several topologies, not exactly thought as DC-DC converters with an intermediate AC link are proposed in [11] and [12].

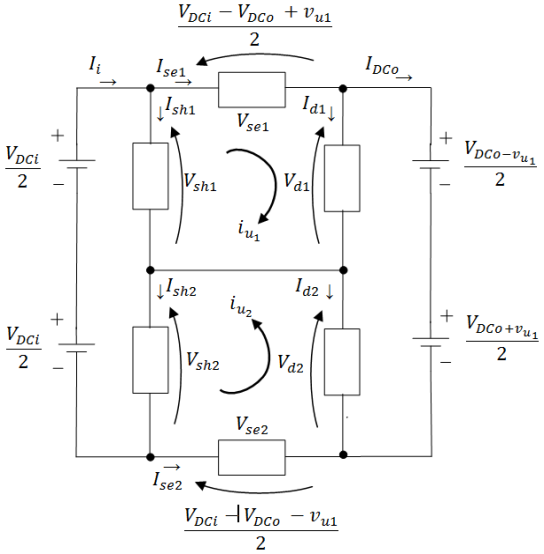

Fig. 1. Proposed DC-DC Multilevel Modular Converter.

In this paper a modular multilevel DC-DC converter is proposed for HVDC applications. The proposed Modular Multi-level DC-DC converter (DC-DC-MMC) topology is based on the topology introduced in [15], which has three MMC branches arranged in a Π topology. The proposed DC-DC converter consists of six branches arranged in a double Π topology, as shown in Fig. 1. Each branch can have N H-bridge converter modules. In comparison to other MMC based DC-DC power converter topologies, such as those using intermediate AC links [4], [9], the DC-DC double Π topology

proposed in this work does not require intermediate coupling transformers and may require smaller silicon area, i.e. summation of volt amp product of power semiconductor devices to implement the overall power converter.

Each Π topology operates in a similar manner. A control system for the total H-bridge DC link energy in every branch is presented, the modeling of any branch with N H-bridge converter is also included. Results showing the behavior of the DC-DC MMC both supplying energy to a DC network and controlling the power flow in a HVDC grid are also presented.

II. Modular Multi-Level DC-DC Converter

One of the main challenges in MMC topologies is to keep the DC voltage capacitor in each cell (either for full or half H-bridge) within certain range in order to operate the power devices safely and ensuring the control of the converter current. The appropriate DC voltage regulation in each cell will ensure the correct operation of the entire branch. The energy balance between the total amount of energy stored in the capacitors in a branch and the energy supplied from those capacitors, within a time window, is a key factor to maintain capacitor voltages within the nominal values [16]-[18]. In other words, the average power shared between each branch and the system has to be, neglecting losses, null.

In [8]-[10], the energy balance is achieved by imposing a current in each branch which contains a component at the intermediate AC frequency f_u and a DC component (in this work, a 500Hz AC signal is used to proof the concept). In this way the total energy stored in a branch can be fully regulated. The topologies in [11], like the one proposed here, do not use an intermediate AC link but they also require an AC voltage and current component to enable converter branches to exchange power, hence energy, with the system at a component other than the DC one. This auxiliary AC component, referred as to secondary frequency component in [11], will provide energy balance at the branch level in the double Π DC-DC topology. The energy balance within a particular branch, i.e. the DC voltage balance in each cell in the branch, can be carried out, for instance, as proposed in [15] or exploiting the commutation redundant states as described in [10] and [18].

The strategy for regulating the H-bridge converter DC link voltage of the proposed DC-DC converter is a two-fold scheme: 1) control of the total energy in every branch of the DC-DC converter topology and 2) balance of the DC link voltage of every H-bridge converter module that forms a branch. Fig. 1 shows the different currents and voltages used for the control of the MML DC-DC converter. In order to control the total energy in each branch of the converter topology; DC and AC circulating currents are used. These currents are imposed in the power converter by a PI and a resonant controller, respectively. The circulating AC current I_{u_1} controls the total energy in the derivation branch. This current component transfers energy to/from the DC side capacitors as given by $\int v_{u1} i_{u1} dt$ (with $v_{u_1} and\ i_{u_1}$ in phase). The voltage v_{u_1}, set by the corresponding branch, cancels out with the other AC voltage in the other Π converter and it does not appear at the output. The currents I_{sh_i} (i=1, 2) controls the corresponding total energy in the i-th shunt branch. The total energy in the series and derivation branches in the top and bottom Π arrangements are controlled by I_{serie1} and I_{serie2} respectively.

The DC voltage balance of the N H-bridge converter modules which form a branch (i.e. the series and parallel branches) is carried out as in [15]. This is by balancing (N-1) capacitor voltage deviations with respect to the average capacitor voltage of the branch. Each voltage deviation is fed into a dedicated PI controller which sets the required balancing voltage component in each H-bridge converter module. This voltage balancing component is in quadrature to v_{u_1}. This facilitates design of the control system since it provides decoupling between the energy balance and DC voltage balancing sub-systems.

The operating principle of the top and bottom Π converter topologies are equivalent, hence only the top half of the full double Π converter is analyzed. The bottom half operates in a similar manner, but with the output AC voltage component shifted 180º, so no AC voltage appears at the total output. In the following equations upper case variables represent DC components and lowercase variables AC components.

Using the voltages and currents defined in Fig 1, it can be shown that the instantaneous power in the series, derivation and shunt branches are given by (1), (2) and (3), respectively:

$$p_{se1} = \frac{dW_{se1}}{dt} = \left(\frac{V_{DCi} - V_{DCo} + v_{u_1}}{2}\right)\left(I_{serie1} + i_{u_1}\right) \quad (1)$$

$$p_{d1} = \frac{dW_{d1}}{dt} = \left(\frac{V_{DCo} - v_{u_1}}{2}\right)\left(I_{serie1} + i_{u_1} - I_{DCo}\right) \quad (2)$$

$$p_{sh1} = \frac{dW_{sh1}}{dt} = \frac{V_{DCi}}{2}\left(I_{sh1} - i_{u_1}\right) \quad (3)$$

where W_{se1}, W_{d1}, and W_{sh1} are the instantaneous stored energy of the series, derivation and shunt branches respectively. v_{u_1} and i_{u_1} are in phase, therefore, average powers for the branches are given by (4), (5) and (6), respectively:

$$\frac{d\bar{W}_{se1}}{dt} = \left(\frac{V_{DCi} - V_{DCo}}{2}\right) \cdot I_{serie1} + \frac{V_{u_1}}{2} \cdot I_{u_1} \quad (4)$$

$$\frac{d\bar{W}_{d1}}{dt} = \frac{V_{DCo}}{2} \cdot (I_{serie1} - I_{DCo}) - \frac{V_{u_1}}{2} \cdot I_{u_1} \quad (5)$$

$$\frac{d\bar{W}_{sh1}}{dt} = \frac{V_{DCi}}{2} \cdot I_{sh1} \quad (6)$$

where $\bar{W}_{se1}$, $\bar{W}_{d1}$, and $\bar{W}_{sh1}$ are the average stored energy of the series, derivation and shunt branches respectively. V_{u1} and I_{u1} are peak values of v_{u1} and i_{u1} respectively. According to (6) I_{sh_1} can be used to control the total energy in the shunt branch. From (5) it can be seen that derivation branch energy can be controlled using i_{u_1}. Adding (4) and (5) yields to:

$$\frac{d\bar{W}_{T1}}{dt} = \frac{d\bar{W}_{se1}}{dt} + \frac{d\bar{W}_{d1}}{dt} = \frac{V_{DCi}}{2} \cdot I_{serie1} - \frac{V_{DCo}}{2} \cdot I_{DCo} \quad (7)$$

Therefore, the total energy in the series and derivation branches can be controlled by adjusting I_{serie1} (I_{DCo} is the output current and can be considered a perturbation). Adjustment of each current component is done in according to its corresponding energy deviation, with respect to its reference value, in a closed loop fashion.

The control structure for the energy control in the shunt branch uses a PI controller. This sets the reference current I_{sh_1}. This current I_{sh_1} is then forced by the shunt branch using an internal current control loop, as depicted in Fig. 2. A resonant controller is used to force the circulation of the AC components through the series branch. The design of the resonant controller follows the approach presented in [19]. The strategy for the energy control in the derivation branch also uses a PI controller; see Fig. 3, which sets the amplitude of circulating current I_{u_1}. Current I_{u_1} is then multiplied by a 500Hz template sinusoidal signal to obtain the circulating reference current i_{u_1}.This current component is forced through the converter by an internal current control which uses a resonant controller. The choice of the frequency for the compensation AC voltage component is a trade-off between converter losses and capacitor requirements, measured in terms of energy storage, hence physical size of capacitors. The higher the frequency of the AC component, the higher the switching losses, hence converter losses, but the smaller the change of energy of DC link capacitors during one cycle of the AC compensation voltage. The total energy in the series and derivation branch, considering the two branches together, is controlled by the adjustment of I_{serie1}. A PI controller processes the energy error and sets this DC reference current component, which, like the AC current component, is imposed in the converter by an internal current control, in this case a PI controller, as shown in Fig. 4.

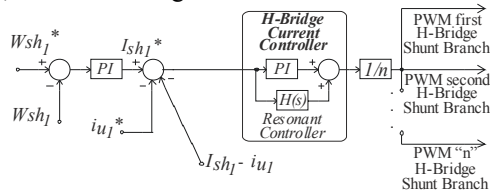

Fig. 2. Shunt branch energy control scheme.

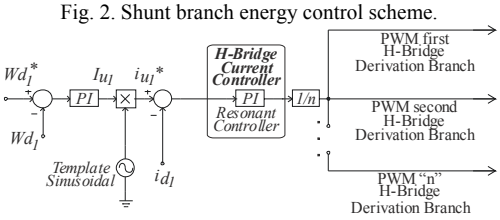

Fig. 3. Derivation branch energy control scheme.

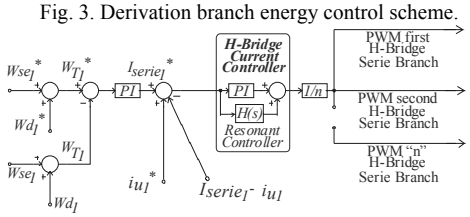

Fig. 4. Total series plus derivation branches energy control scheme.

III. Modelling of N Level DC-DC Converter

A simplified model is developed to simulate a DC-DC converter of any number of levels (see Fig. 5). The N series-connected cells of each arm are replaced by a single voltage source (V_{eq}) and a resistor (R_{eq}) where the following simplifications are considered:

- The diodes and IGBTs are modeled as a two-state resistance: R_{ON} and R_{OFF}. The value of the off-state resistance is considered to be infinite.
- Cells have three possible states: positive output voltage (1), negative output voltage (-1) and zero output voltage (0).
- The values of the equivalent voltage source and resistance of each arm are:

$$R_{eq} = \sum_{i=1}^{N} R_{eq}^{SM}(i) \quad (8)$$

$$V_{eq} = \sum_{i=1}^{N} state(i) \cdot V_c(i) \quad (9)$$

where state(i) is an array containing the state of each cell. The state of each cell is given by the modulation technique and the voltage reference from the control algorithms. The voltages of every cell capacitor are computed at each simulation step and the values of R_{eq} and V_{eq} are updated. Further details can be found in [20].

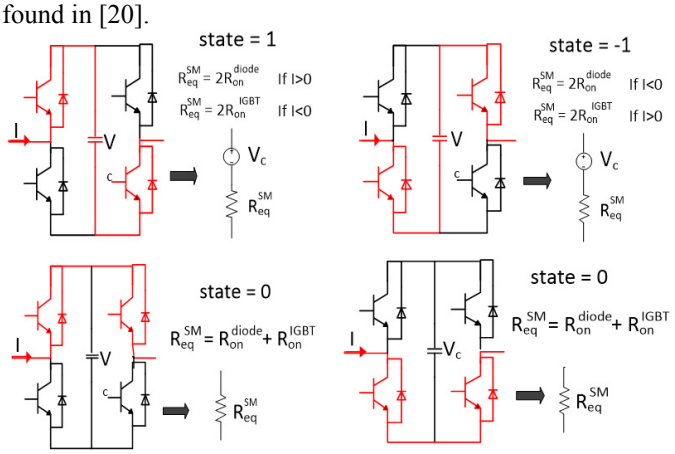

Fig. 5. Simplified model for N MMC's.

IV. Results For Power Flow In HVDC Systems

The operation of the proposed converter has been validated by considering the system in Fig. 6. The rating of the power converter depends on the voltage ratio of the MMC DC-DC converters; hence this is certainly an issue to bear in mind and depends on the application. In all cases, a converter with 150 cells in each one of the branches is considered. Each cell has a capacitor of 3000uF and the cell average voltage is 2.5kV.

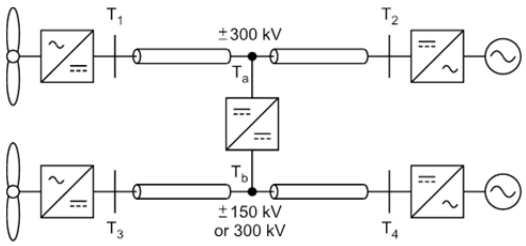

Fig. 6. Schematic of interconnected HVDC grid.

A. Power flow for HVDC lines with different voltage level

Figs 7 and 8 show the steady state operation of the MMC-DC-DC converter when delivering 200MW to the ±150kV

grid. Fig. 7 shows the output voltage, converter branch currents and converter output current. Fig. 8 shows the average, maximum and minimum cell voltages in each one of the converter branches. Fig. 9 shows system operation when the MMC-DC-DC converter power reference is ramped down from 200MW to -200MW. Voltages at busses T2 and T4 are being held constant by the respective converters. Initially, the DC-DC converter is delivering 200MW from Ta to Tb. The 200MW are delivered by T2 converter stations (150MW) and by the wind farm T1 (50MW). No wind power is delivered by wind farm T3, hence, the 200MW injected by the DC-DC converter are absorbed by converter T4. At t=0.2, the power reference to the DC-DC converter is ramped down, to achieve full power reversal in 1s. Such a fast power reversal might not be realistic, as might be too fast for the size of the considered system. However, it is useful to show the dynamic performance of the DC-DC converter. As the power transferred from Ta to Tb decreases, power delivered by the T2 converter also decreases, therefore, the power absorbed by the T4 converter also decreases. At t=0.5 power reversal occurs and converter T4 injects power to the HVDC grid while T1 absorbs power from the HVDC grid. At t=1.4s wind farm T1 stops injecting power and windfarm T3 starts injecting power to the HVDC grid. The MMC DC-DC converter keeps the power flowing from Ta to Tb to -200MW and powers flowing to and from T2 and T4.

The voltage traces in Fig. 9 shows the input and output voltages of the MMC-DC-DC converter during the power flow change. The average cell capacitor voltage and arm currents are shown in Fig. 10. Clearly, cell voltages in the input shunt branch remain close to their 2.5kV reference, whereas the cell voltages of the series and output derivation branches depart from their steady state value due to the ramped change in reference power. This effect can be easily reduced by means of current reference feed-forward compensation. In any case, note that cell voltage deviation is within reasonable limits and in opposite directions, leading to constant total energy in series and derivation branches, as expected from theory.

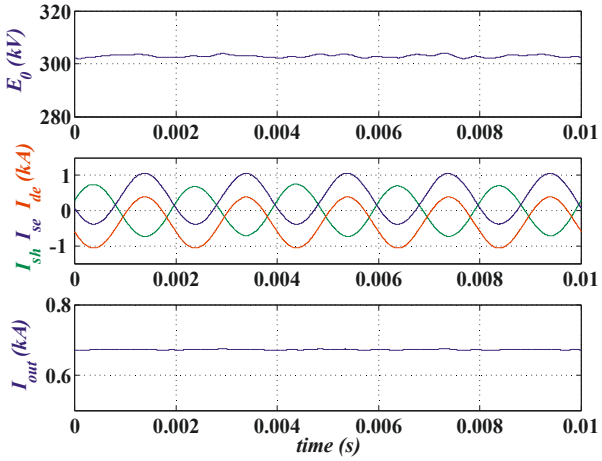

Fig. 7. Steady state operation when delivering 200MW.

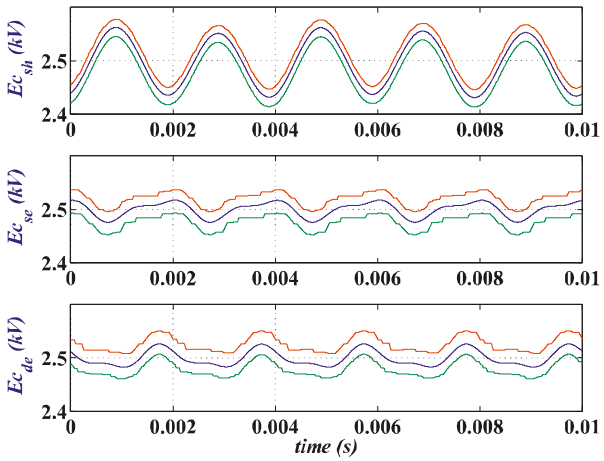

Fig. 8. Cell voltages when delivering 200MW.

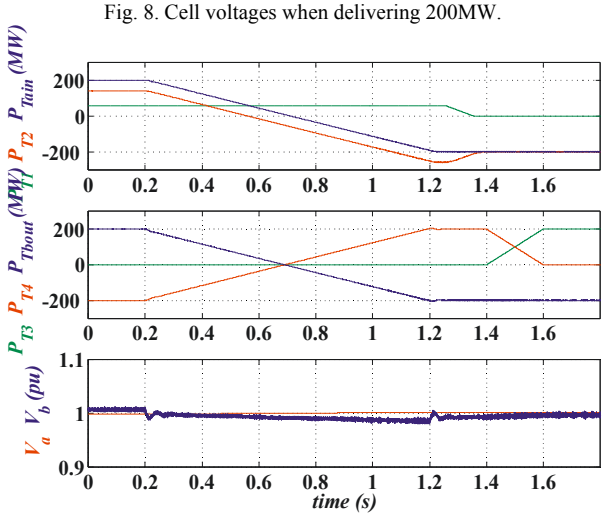

Fig. 9. Results for 200 MW power reversal.

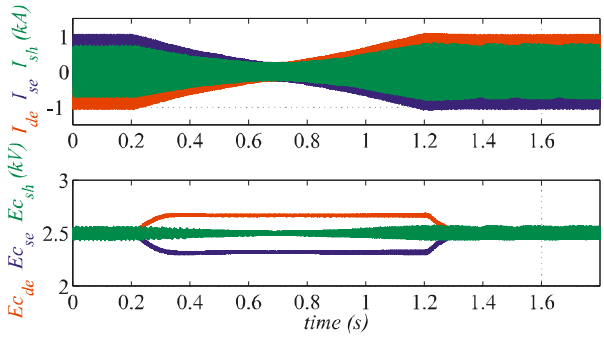

Fig. 10. Arm currents and voltages during power reversal.

Fig. 11 shows the operation of the MMC-DC-DC converter when delivering -200MW, note that the dc components of I_{se} and I_{de} have just changed their sign with respect to those in Fig. 7, again, as expected from the theory.

B. Power flow for HVDC lines with same voltage level

The MMC DC-DC power converter is used to interconnect two HVDC ±300kV line. Fig. 12 shows a power transient between the +-300kV lines. Initially, the DC-DC converter is delivering 600MW from Ta to Tb. The 600MW are delivered by the wind farm T1 (50MW), and the rest is delivered by the T2 converter. At this stage, no wind power is delivered by wind farm T3, hence, the 600MW injected by the DC-DC converter are absorbed by converter T4. At t=0.2, the power

reference to the DC-DC converter is ramped down, to achieve full power reversal in 1s. Such a fast power reversal might not be realistic, as might be too fast for the size of the considered system. However, it is useful to show the dynamic performance of the DC-DC converter. As the power transferred from Ta to Tb decreases, power delivered by the T2 converter also decreases, therefore, the power absorbed by the T4 converter also decreases. At t=0.5 power reversal occurs and converter T4 injects power to the HVDC grid while T1 absorbs power from the HVDC grid.

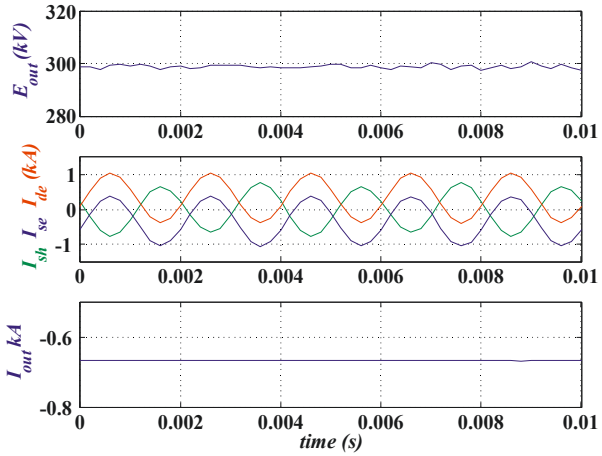

Fig. 11. Steady state operation when delivering -200MW.

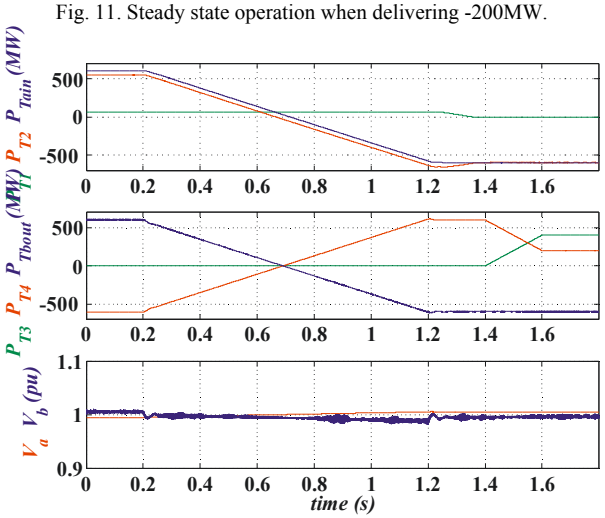

Fig. 12. Power transient between the +-300 kV lines.

At t=1.4s wind farm T1 stops injecting power and wind farm T3 starts injecting power to the HVDC grid. The MMC DC-DC converter keeps the power flowing from Ta to Tb to -600MW and powers flowing to and from T2 and T4. The voltage trace shows the input and output voltages of the MMC-DC-DC converter during the power flow change. Fig. 13 shows the branch currents and cell voltages during power reversal.

Branch currents on the top graph consist on a circulating AC current plus a DC component. The DC component on I_{se} does clearly change during the transient, whereas the DC component of the other branches is almost negligible. Note the average capacitor cell voltages depart very little from their references even in the presence of a large power transient.

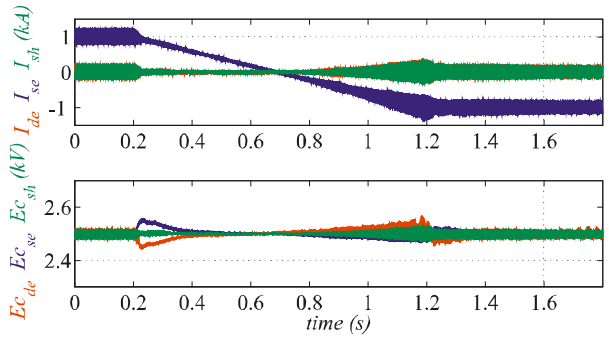

Fig. 13. Branch currents and cell voltages during the power reversal.

Figs. 14 and 15 show the details of currents and voltages when delivering 600MW and -600MW respectively. In both cases the output voltage is kept at 600 kV (+-300 kV). Both I_{sh} and I_{de} are equal to the considered circulating current (0.25 pu peak). On the other hand, I_{se} shows the circulating current on the top of the 1kA reference. Fig. 16 shows the average, maximum and minimum cell capacitor voltages in shunt, series and derivation branches when delivering 600MW (traces are the similar with a reference of -600MW). Average voltages are centred about 2.5kV, with low variation.

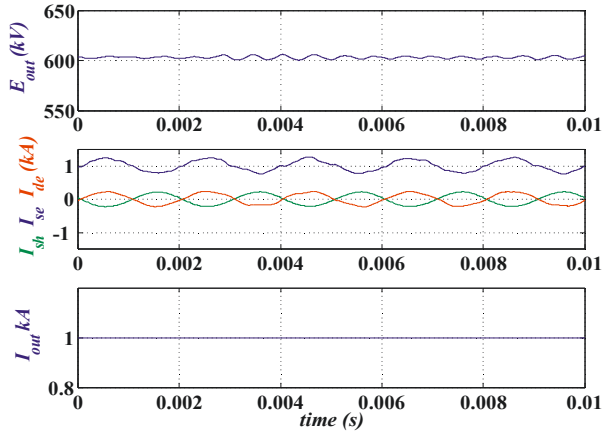

Fig. 14. Detail of voltages and currents with delivering 600MW.

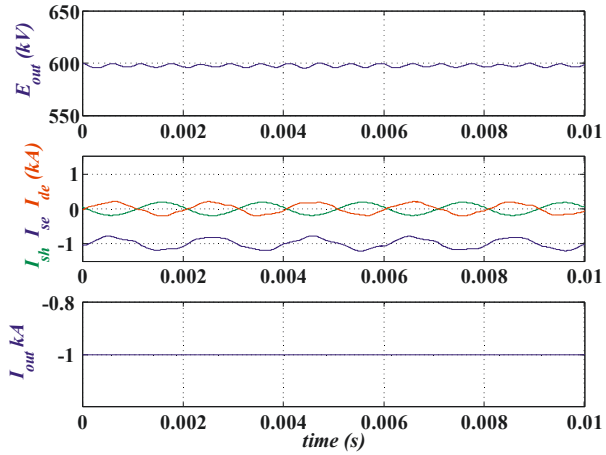

Fig. 15. Detail of voltages and currents with delivering -600MW.

C. *Discussion on sizing of the converter*

For the proposed MMC DC-DC converter application, a 4.5kV/1.2kA IGBT [21] could be considered as a suitable switching device for H-bridges with a DC link working

voltage of 2.5kV and maximum current of 1.0kA. For the ±300kV to ±150kV application, a suitable value for the peak value of V_u is 150kV. Considering the energy balance (series and derivation) and the maximum cell current (1.0kA), the maximum series branch DC and AC circulating current (under normal operation conditions) will be 0.33kA and 0.67kA, respectively. Therefore, the power rating (nominal power) of the converter is 2×300 kV×0.33kA = 200MW. The number of cells per branch can be calculated as the number of cells to produce nominal maximum branch voltage with a 20% security margin. This accounts for the cell capacitor voltage ripple (less than 5% in the case studied) and sufficient DC link voltage to force the circulating current. According to this, 150 H-bridges are required for a 300 kV branch. The branch inductor was chosen so that it yields an AC voltage of 10% of the circulating voltage (V_u) when the DC-DC converter operates at nominal power. This operation condition requires the largest AC circulating current, 0.67kA peak in this case (defined as the nominal circulating current). The cell capacitor is chosen to limit the voltage ripple to ±5% under all operation conditions; although a lower capacitance can be used because of the device voltage rating.

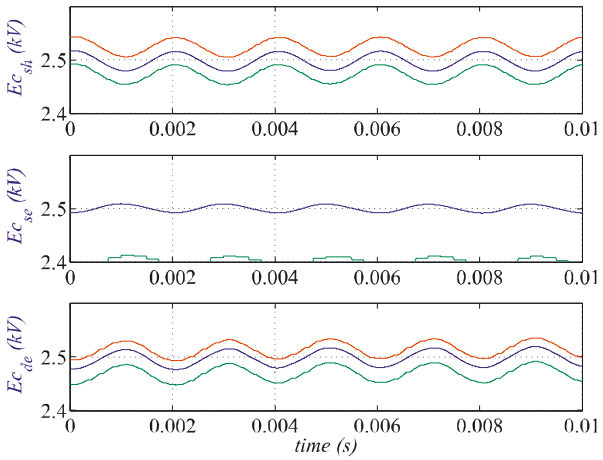

Fig. 16. Average, maximum and minimum cell capacitor voltages in shunt, series and derivation branches when delivering 600MW.

V. Conclusions

This paper has presented a novel Modular Multi-Level Converter topology for DC-DC converters suitable for interconnecting HVDC lines and exerting power flow control in HVDC power systems. The proposed topology does not require the use of high frequency, high voltage transformers.

A suitable control strategy has been proposed for the aforementioned DC-DC converter, for both the arm energy control and module capacitor balance. The technical viability of the proposed MML DC-DC converter and control strategy has been thoroughly validated by means of detailed simulations considering a significant number of H-bridge modules per branch.

Acknowledgments

The support of Fondecyt grant 1151325, CONICYT/FONDAP/15110019, the Spanish Ministry of Economy Grant DPI2014-53245-R, University La Frontera grant DIUFRO09-0037 and Universitat Jaume I grants P1·1B2013-51 and E-2014-24 is kindly acknowledged.

References

[1] D. Jovcic, "Interconnecting offshore wind farms using multiterminal VSC-based HVDC," in *Power Engineering Society General Meeting, 2006. IEEE*, 2006.

[2] S. Allebrod, R. Hamerski, and R. Marquardt, "New transformerless, scalable Modular Multilevel Converters for HVDC-transmission," in *Power Electronics Specialists Conference, 2008. PESC 2008. IEEE*, 2008, pp. 174–179.

[3] Y. Wang and R. Marquardt, "Future HVDC-grids employing modular multilevel converters and hybrid DC-breakers," in *2013 15th European Conference on Power Electronics and Applications*, 2013, pp. 1–8.

[4] A. Lesnicar and R. Marquardt, "An Innovative Modular Multilevel Converter Topology Suitable for a Wide Power Range", IEEE PowerTech Conference, Bologna, Italy, June 23-26, 2003.

[5] T. Westerweller et al, "Trans Bay Cable- world's first HVDC system using multilevel voltage-source converter", CIGRE Paper B4-101, Paris, 2010.

[6] N. Flourentzou, V.G. Agelidis, G.D. Demetriades, "VSC-based HVDC power transmission systems: An overview", IEEE Trans. Power Electr. 2009, 24, 592-602.

[7] H. Akagi, "Classification, Terminology, and Application of the Modular Multilevel Cascade Converter (MMCC)", IEEE Transactions on Power Electronics, vol. 36, no. 11, pp. 3119-3130, November 2011.

[8] S. Kenzelmann, A. Rufer, M. Vasiladiotis, D. Dujic, F. Canales and Y. R. de Novaes, "A versatile DC-DC converter for energy collection and distribution using the Modular Multilevel Converter", EPE 2011, Birmingham, pp. 1 –10.

[9] Montesinos-Miracle, D., Massot-Campos, M., Bergas-Jane, J., Galceran-Arellano, S., Rufer, A., "Design and Control of a Modular Multilevel DC/DC Converter for Regenerative Applications", Transactions on Power Electronics, vol 28, no. 8, pp 3970-3979, 2013.

[10] Luth T., Merlin M.M.C., Green T.C., Hassan, F., Barker C.D., High-Frequency Operation of a DC/AC/DC System for HVDC Applications , IEEE Trans. on Power Electronics, vol.29, no.8 , 2014 , pp. 4107 – 4115.

[11] J. A. Ferreira, "The Multilevel Modular DC Converter" IEEE Trans. on Power Electronics, Vol. 28, pp 4460-4465, 2013.

[12] Norrga, S.; Angquist, L.; Antonopoulos, A. "The polyphase cascaded-cell DC/DC converter", Energy Conversion Congress and Exposition (ECCE), 2013 IEEE, On page(s): 4082 – 4088.

[13] D Jovcic and B.T Ooi, "Developing DC transmission network using DC transformers" IEEE Transactions on Power Delivery, Vol. 25, issue 4, October 2010, pp 2535-2543.

[14] C. D. Barker, C. C. Davidosn, D. R. Trainer and R. S. Whitehouse, "Requirements of DC-DC converters to facilitate large DC grids", Cigre, SC B4 HVDC and Power Electronics, 2012.

[15] D. Soto-Sanchez, R. Pena, R. Cardenas, J. Clare, P. Wheeler, "A Cascade Multilevel Frequency Changing Converter for High Power Applications", IEEE Trans. On Industrial Electronics, Vol. 60, pp 2118-2130, 2013.

[16] M. Hagiwara and H. Akagi, "Control and Experiment of Modular Multilevel Converters", IEEE Transactions on Power Electronics, vol. 24, no. 7, pp. 1737-1746, July 2009.

[17] A. Antonopoulos, L. Angquist and H.-P. Nee, "On dynamics and voltage control of the Modular Multilevel Converter," EPE 2009.

[18] M. Saeedifard and R. Iravani, "Dynamic performance of a modular multilevel back-to-back HVDC system", IEEE Trans. Power Del., vol. 25, no. 4, pp. 2903–2912, Oct. 2010.

[19] P. Lezana, C. Silva, J. Rodriguez, M. Perez , "Zero Steady State Error Input Current Controller for Regenerative Multilevel Converters Based on Single-Phase Cells "IEEE Trans. On Industrial Electronics, Vol. 54, N° 2, pp 773-740, April 2007.

[20] R. Vidal-Albalate *et al,* "Simplified Model for Modular Multi-Level Converter Simulation," Proc. of the 11th International Conference on Modeling and Simulation of Electric Machines, Converters and Systems, Valencia, 2014, pp. 487–492.

[21] Datasheet Infineon FZ1200R45KL3 IGBT, [Online], available: http://www.infineon.com/dgdl/Infineon-FZ1200R45KL3_B5-DS-v03_00-en_de.pdf.